Resonance patterns of an antidot cluster: From classical to quantum ballistics

G. Kirczenow
Department of Physics, Simon Fraser University, Burnaby, British Columbia, Canada V5A 1S6

B. L. Johnson
Department of Physics and Astronomy, University of New Mexico, Albuquerque, New Mexico 87131-1156

P. J. Kelly
Institute for Microstructural Sciences, National Research Council, Ottawa, Canada K1A 0R6

C. Gould
Institute for Microstructural Sciences, National Research Council, Ottawa, Canada K1A 0R6
and Université de Sherbrooke, Sherbrooke, Québec, Canada J1K 2R1

A. S. Sachrajda, Y. Feng, and A. Delage
Institute for Microstructural Sciences, National Research Council, Ottawa, Canada K1A 0R6
(Received 10 June 1997)

We explain the experimentally observed Aharonov-Bohm (AB) resonance patterns of an antidot cluster by means of quantum and classical simulations and Feynman path integral theory. We demonstrate that the observed behavior of the AB period signals the crossover from a low B regime which can be understood in terms of electrons following classical orbits to an inherently quantum high B regime where this classical picture and semiclassical theories based on it do not apply. [S0163-1829(97)05036-4]

I. INTRODUCTION

In recent years the physics of electrons in semiconductor systems of reduced dimensionality has been studied extensively at high magnetic fields where the quantum mechanics of Landau levels gives rise to the quantum Hall effect, and also at very low magnetic fields where many phenomena can be understood in terms of electrons following classical ballistic trajectories.[1] The crossover between these two very different regimes is poorly understood; identifying and performing relevant experiments has been difficult and simple theoretical models that capture the essential physics have not been formulated.

A series of experiments carried out recently in the crossover regime have yielded intriguing results.[2] The device studied (see the left inset of Fig. 1) was a quantum wire defined in a two-dimensional electron gas and containing a pair of antidots, i.e., regions from which electrons are excluded, in close proximity to each other. As a function of magnetic field B, the conductance G of this device showed a dip associated with the trapping of electrons in a closed orbit encircling the antidot pair.[3] Superimposed on this dip were Aharonov-Bohm (AB) conductance oscillations due to quantum interference associated with the multiply connected device geometry. Plot (a) at the bottom of Fig. 1 is an example of such an experimental conductance trace. Within experimental uncertainty, the period of the AB oscillations was *independent* of B,[2] a phenomenon that has been difficult to understand since the area enclosed by a classical cyclotron orbit decreases as B increases. One might expect this to result in an AB period that increases with B.[4] Another intriguing experimentally observed phenomenon that will be reported here is that when the geometry of the antidots is varied smoothly by varying the voltage on the gates that define them, an additional AB conductance peak can, under certain conditions, appear abruptly, as if the electronic orbit suddenly enclosed an extra quantum of magnetic flux. As the gate voltage is varied further, the sequence of AB resonances (as a function of B) soon reforms and becomes regular again. Such dislocations in the pattern of AB resonances are observed when more than one transverse mode is transmitted through the constrictions between the antidots and the edges of the quantum wire. The independence of the AB period of the value of B is observed both in this regime and when only a single mode is transmitted.

This is clearly an ideal system for comparing classical and quantum behavior. In this paper we account for its surprising behavior with the help of computer simulations and Feynman path integral theory. Our quantum simulations reproduce the experimentally observed conductance dip and AB resonances. We show the latter to be due to resonant transmission (as distinct from resonant reflection) of electrons. We demonstrate that the experimentally observed constancy of the AB period is an innately quantum phenomenon that signals the *breakdown* of the semiclassical picture of electrons following classical trajectories that is valid at lower B. By contrast, *no* breakdown of the semiclassical picture has been found in previous work on large arrays of antidots[7] because in those devices[3] the constrictions were much wider, each transmitting many modes. Our quantum simulations also reproduce the experimentally observed abrupt appearance of additional AB resonances as the antidot geometry is varied and the subsequent reemergence of the regular se-

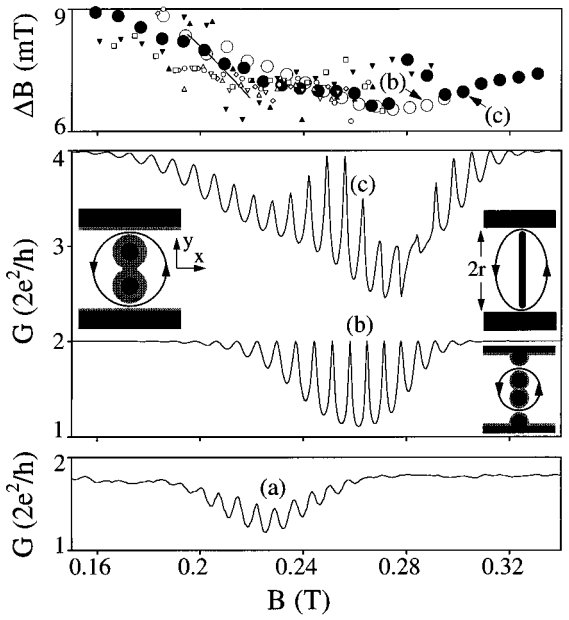

FIG. 1. Two-terminal conductance G and AB period ΔB vs B for the device in left inset. Plot (a) $[(b)]$: experiment (quantum simulation) with one mode transmitted through each constriction. Plot (c): quantum simulation with two modes transmitted. Large open (full) circles: ΔB for case (b) $[(c)]$. Small open (full) symbols: experimental ΔB in one (two) mode regime. Solid line in top panel: semiclassical ΔB vs B for closed classical orbit of antidot pair; $s_d=2.0$. Left inset: Schematic of quantum wire with two antidots. Black and shaded regions are depleted of electrons. Upper right inset: Simplified model used in analytic path integral theory. Lower right inset: Device in which the straight edges of the wire are further from the constrictions.

quence of conductance peaks; an explanation of this phenomenon is also suggested.

II. THE MODEL

The model used in our quantum simulations is a tight-binding Hamiltonian on a square lattice,

$$H=\sum_{m,n} a^{\dagger}_{mn}a_{mn}W_{mn}-t(a^{\dagger}_{m+1n}a_{mn}e^{in\alpha}+a^{\dagger}_{mn}a_{m+1n}e^{-in\alpha} + a^{\dagger}_{mn+1}a_{mn}+a^{\dagger}_{mn}a_{mn+1}). \quad (1)$$

Here m and n label sites in the x and y directions in Fig. 1, $t=\hbar^2/(2m^*d^2)$, $\alpha=eBd^2/\hbar$ [the magnetic phase factor $e^{in\alpha}$ is associated with hopping in the x direction since we use the Landau gauge $\mathbf{A}=(-By,0,0)$ (Ref. 8)], $\mathbf{B}$ points in the z direction, d is the lattice parameter, $-e$ is the electron charge, and m^* is the electron effective mass. We ignore the small Zeeman splitting between spin up and down. The electron potential energy [the site energy W_{mn} in Eq. (1)] was assumed to be parabolic near the edges of the gates that define the boundaries of the wire and the antidots, and flat elsewhere. W_{mn} was modeled as a sum of partial electron potential energy functions $W_g(u)$ associated with the individual gates g, with $W_g(u)=E_F[u-a(1+s_g)]^2/a^2$ for $u<a(1+s_g)$ and $W_g(u)=0$ for $u>a(1+s_g)$. u is the distance from the edge of the gate. a is a scale of length that was chosen to be 0.05μ. s_g is the dimensionless width of the depleted region around the gate. (In this work $s_g=1$ for both gates that define the edges of the quantum wire and $s_g\equiv s_d$ for both gates that define the antidots.) $E_F=\pi n\hbar^2/m^*$ is the electron Fermi energy measured from the bottom of the band and $n=3.47\times10^{-15}\ \mathrm{m}^{-2}$ is the 2D electron density far from the gates. As in the experiments, the distance between the outer gates that define the quantum wire in Fig. 1 was 1μ, each antidot had a lithographic diameter of 0.2μ, and the spaces between the two antidots and between the antidots and outer wire gates were 0.2μ. In our simulations 100 lattice sites spanned the 1μ width of the wire. For a typical value of $B=0.25$ T this implies five lattice spacings d per magnetic length $(\hbar/(Be))^{1/2}$. Thus although our numerical results reproduced the experimentally observed behavior of the device quite well, it should be emphasized that the model of the system used was a moderately coarse tight-binding lattice rather than a continuum.[9]

III. QUANTUM SIMULATIONS AND COMPARISON WITH EXPERIMENTS

The electron wave functions and the multichannel quantum transmission and reflection matrices for the above model were calculated numerically using a stabilized transfer matrix technique.[10] The two-terminal conductance G was then obtained from the Landauer formula[11] $G=(e^2/h)\mathrm{Tr}(\mathbf{tt}^{\dagger})$.

The calculated conductance G of the device is shown in Fig. 1 for two values of the width of the depleted regions around the antidots. Plot (b) $[(c)]$ is for $s_d=2.050$ (1.850) for which the *individual* conductances G_1 of the two constrictions between the antidots and the outer gates are both accurately quantized to $2e^2/h$ $(4e^2/h)$; i.e., one (two) transverse modes are transmitted perfectly through each constriction. The constriction between the antidots is pinched off. At the upper and lower ends of the range of B shown, the conductances of the two parallel constrictions are added [as at $B=0$ (Ref. 12)] and the conductance of the device is close to $G=4e^2/h$ $(8e^2/h)$. However, in between G is depressed; this is the dip in the conductance of the device that is observed experimentally[2] due to the trapping of electrons in the orbit around the antidots. This effect is remarkably strong—near the center of the dip the calculated conductance falls to little more than half of its maximum value. As in the experimental data, the calculated G exhibits AB oscillations superimposed on the conductance dip, and as in the data the pattern of oscillations is much simpler when only one mode is transmitted through each constriction. [The experimental trace (a) is in the single mode regime as is plot (b).] The conductance dip in the simulations is at a somewhat higher value of B than in the experiment; we did not tune the model parameters for a perfect match. This should be remembered when comparing simulations with experiment in Fig. 2 and in the top panel of Fig. 1.

A feature of our numerical results is that the AB resonances (when they are strong) usually take the form of sharp peaks and smooth minima in the conductance; in the simpler case (b) the peak conductance equals the ideal value $4e^2/h$ for perfect transmission through both constrictions. This means the AB resonant states give rise to *resonant transmission.* Trace (a) is consistent with what would be obtained by

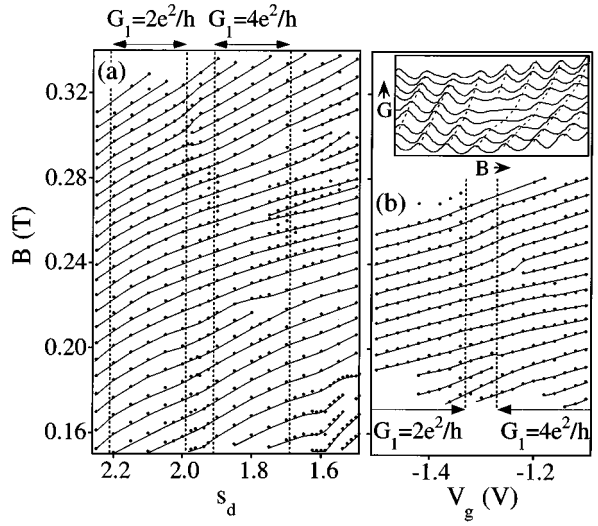

FIG. 2. Positions in B of conductance maxima obtained from (a) quantum simulations vs width s_d of the antidot depletion regions and (b) measurements vs antidot gate voltage V_g. Quantized plateaus in conductance G_1 of *individual* constrictions are indicated. Curves are guides to the eye. Inset: Measured conductance G [for various V_g from -1.16 V (top trace) to -1.32 V] vs B (from 0.21 T to 0.26 T) around dislocation at $V_g=-1.22$ V, $B=0.237$ T. Traces are offset for clarity.

broadening a series of peaks with sharp maxima and smooth minima like those in plot (b); no kT broadening is included in plots (b) and (c).

The locations in B of the peaks in the calculated conductance G are shown in Fig. 2(a) for various widths s_d of the antidot depletion regions. The results in Fig. 2(a) are in good qualitative agreement with the corresponding experimental data plotted against the antidot gate voltage V_g in Fig. 2(b). In both the experiment and simulations the pattern of conductance maxima is simple and regular when one mode is transmitted through each of the two constrictions $(G_1=2e^2/h)$. But in the regime where two modes are perfectly or partly transmitted there are anomalies—a conductance maximum disappears as s_d increases near $(s_d=1.8, B=0.216$ T) and as s_d decreases near $(s_d=1.97, B=0.30$ T). But as s_d is varied further the remaining conductance peaks form into a periodic pattern once again; i.e., these anomalies resemble dislocations in a crystal. The same two dislocations are seen at somewhat lower B in the experimental data when two modes are transmitted through each constriction.[13] A series of experimental conductance traces around the dislocation at $B=0.237$ T is shown in the inset of Fig. 2(b). Note that in the dislocation found experimentally on the high (low) B side of the trapping dip in the conductance, the conductance peak disappears as the antidot gate voltage becomes more (less) negative. This is in agreement with the orientation of the corresponding dislocations in Fig. 2(a) since increasing the depletion width s_d in the simulations means making V_g more negative.

Since the dislocations in the pattern of AB resonances are found in our simulations that are based on a model of noninteracting electrons, it seems unlikely that they are due to electron-electron interactions. However, both experimentally and in the simulations the dislocations occur when more than one mode is transmitted through the constrictions. Indeed more complex dislocation patterns are seen in Fig. 2(a) for $s_d<1.7$, where a third mode is transmitted. More than one mode penetrating the constrictions should result in more than one trapped electron orbit of the antidot pair being present. This is consistent with the beatlike modulation of the amplitude of the AB resonances visible in plot (c) of Fig. 1 (two modes transmitted), but absent in plot (b) (one mode penetrates). Our numerical study of the transmission probabilities associated with *individual* scattering channels that contribute to the total conductance of the device showed that when two modes are transmitted through the constrictions the resonant structures in the different channels fall into two groups. The peaks in the transmission belonging to these two groups move out of phase with each other in the vicinity of the dislocations and cancel there resulting in the disappearance of a conductance peak. Thus it appears that destructive interference of out of phase resonances associated with at least two different orbits is responsible for the dislocations.

The spacing of successive conductance peaks in B (the AB period ΔB) found in the quantum simulations is shown by the large open (full) circles at the top of Fig. 1 for the same s_d as in conductance plot (b) $[(c)]$. ΔB decreases with increasing B at low B but is *stationary* at the conductance dip. [The anomaly in ΔB at $B=2.8$ T for case (c) is due to a dislocation whose core is at $(s_d=1.65,\ B=3.0$ T) in Fig. 2(a).] Since ΔB could only be measured in a relatively narrow range of B at the conductance dip, the fact that the simulations show ΔB to be stationary there accounts for the independence of ΔB of B that was observed by Gould *et al.*[2] The small symbols in the top panel of Fig. 1 show the measured ΔB for several values of V_g. The data shows some scatter but there is overall agreement with the quantum simulations—the measured ΔB also decreases with increasing B at low B and levels out at the conductance dip. Notice that overall ΔB is insensitive to s_d in both Fig. 1 and Fig. 2(a), consistent with the insensitivity to the antidot gate voltage found experimentally.[2]

IV. ANALYSIS: QUANTUM SIMULATIONS VS CLASSICAL SIMULATIONS AND FEYNMAN PATH INTEGRAL THEORY

The fact that ΔB *decreases* with increasing B at low B may at first seem surprising since the area enclosed by a cyclotron orbit in free space decreases with increasing B. However, at low B the diameter of a cyclotron orbit is larger than the distance between the gates defining the edges of the wire, so that a closed *circular* orbit enclosing the antidots cannot occur. But the constrictions between the the gates and the antidots are asymmetric; one side is curved, the other straight—see left inset, Fig. 1. This results in the electron wave, as it emerges from the constriction, being collimated at an angle of about $\pi/6$ relative to the edge of the straight gate[14] so that a closed *noncircular* quantum orbit of the antidots can form.

A similar collimation effect also occurs classically,[14] making closed classical low B orbits possible. We have performed classical calculations of such closed orbits for the same model electron potential as was used in our quantum simulations and calculated the AB phase associated with

these orbits using the semiclassical result $\hbar\phi_{\mathrm{AB}}^{\mathrm{S.C.}}=\oint m^*\mathbf{v}\cdot d\mathbf{l}-eA_eB$. Here A_e is the area enclosed by the orbit. The semiclassical AB period thus obtained for a closed classical orbit is shown by the line in the top panel of Fig. 1; the semiclassical AB period decreases with increasing B as in the quantum simulations but does *not* become stationary.[15] Since the same electron potential energy function was used in both the quantum and classical simulations, the fact that the stationary AB period was only found in the quantum simulations is significant: It implies that the constant AB period observed experimentally is an inherently quantum phenomenon that signals the breakdown of the semiclassical picture of electrons following classical trajectories that is valid at lower B.

One can understand the effect of the confinement of the electron orbit by the edges of the quantum wire on the AB period at low B by considering a simplified model of the device and a class of Feynman paths depicted in the upper right inset of Fig. 1. The edges of the wire are represented by infinite hard walls and the antidots by a narrow infinite barrier. In the symmetric gauge $A=(-By/2,Bx/2,0)$, we parametrize the Feynman path by $x=k(v/\omega)\cos(\omega t)$, $y=(v/\omega)\sin(\omega t)$, where t is the time, v is the Fermi velocity, and $\omega=v/r$. r is half of the distance between the constrictions. k is the parameter that defines the shape of the particular Feynman path. The action for a closed path is then given by $S_k=\oint L\,dt=Tm^*v^2(k^2-2k\omega_c/\omega+1)/4$, where $T=2\pi/\omega$ and $\omega_c=e|B|/m^*$. The action is stationary with respect to the shape parameter k for $k=\hat{k}=\omega_c/\omega$. Thus the stationary Feynman path is circular as expected when $\omega_c=\omega$, i.e., when the cyclotron radius equals r. For lower B, $\omega_c<\omega$ and therefore $\hat{k}<1$ and the stationary Feynman path is an ellipse whose area *increases* as the B increases. This suggests that the AB period should decrease with increasing B, qualitatively in agreement with our low B simulation results. On closer inspection, this turns out to be correct—the propagator $U(\mathbf{r},t,\mathbf{r},t+T)$ for the set of Feynman paths enclosing the barrier is dominated by $e^{iS_{\hat{k}}/\hbar}$, and therefore the AB phase is given (up to a constant) by $\phi_{\mathrm{AB}}\approx S_{\hat{k}}/\hbar=Tm^*v^2(1-\omega_c^2/\omega^2)/(4\hbar)$. The AB period is then given by $2\pi=|\Delta\phi_{\mathrm{AB}}|\approx\Delta B|d\phi_{\mathrm{AB}}/dB|$ or $\Delta B\approx 4\hbar m^*\pi\omega^2/(BTv^2e^2)$; i.e., ΔB decreases as B increases. More general path integral calculations that confirm this qualitative result will be presented elsewhere.

At higher B the cyclotron diameter becomes smaller than the width of the quantum wire, so that the confinement of the AB orbit by edges of the quantum wire should be less important. Thus at higher B one should expect the area of the quantum AB orbit to shrink and the AB period to *increase* with increasing B. The crossover to this higher B regime should occur when the cyclotron diameter is equal to the distance between the two constrictions at the edges of the device, i.e., within the dip in the conductance of the device that is due to the trapping of electrons in the orbit encircling the antidots. This explains why the AB period in our quantum simulations begins to increase with increasing B at the high B edge of the resistance peak, as can be seen in Fig. 1. Thus ΔB was effectively independent of B in the experimental data of Gould *et al.*[2] because that data was taken at the crossover from the low B regime to the high B regime, which coincides with the trapping dip in conductance.[16]

As a further test of this explanation we carried out quantum simulations of transport in a similar device in which the straight edges of the quantum wire are further from the constrictions and should have less of an effect on the AB orbit at the lower values of B. This device is depicted in the lower right inset of Fig. 1. As expected from the above argument, in our simulations of this device the AB period increased with increasing B throughout the range of B in which AB conductance oscillations were present. Experiments by Hirayama and Saku[17] on such a device also found the AB period to increase with increasing B, lending further support to the above theory.

V. CONCLUSIONS

In conclusion, we have shown that the observed Aharonov-Bohm resonance patterns of an antidot cluster can be accounted for by quantum simulations and have demonstrated that the previously unexplained constant period of the resonances signals the crossover from a classical ballistic regime at low magnetic fields to an inherently quantum regime at higher fields. The crossover from classical to quantum ballistics should be an interesting new field of study.

ACKNOWLEDGMENTS

We thank Richard Akis for a helpful suggestion. This work was supported by the NSERC of Canada.

[1] For reviews see *The Quantum Hall Effect*, edited by R. E. Prange and S. M. Girvin (Springer-Verlag, New York, 1990); S. E. Ulloa, A. MacKinnon, E. Castaño, and G. Kirczenow, in *Handbook of Semiconductors*, edited by P. T. Landsberg (North-Holland, Amsterdam, 1992), Vol. 1.

[2] C. Gould *et al.*, Phys. Rev. B **51**, 11 213 (1995).

[3] Such trapping has also been observed in antidot lattices by D. Weiss *et al.*, Phys. Rev. Lett. **66**, 2790 (1991); **70**, 4118 (1993); F. Nihey and K. Nakamura, Physica B **184**, 398 (1993); C. G. Smith *et al.*, J. Phys.: Condens. Matter **2**, 3405 (1990).

[4] Approximately B-independent AB periods also occur in narrow rings (see Ref. 5) and for single antidots in the edge state regime at higher magnetic fields (see Ref. 6). In those cases the constancy of the AB period is a consequence of the entire electron trajectory being tightly constrained by the confining potential of the device so that area enclosed by the electron orbit is nearly independent of the magnetic field. However this simple explanation does not apply to the antidot cluster experiments of Gould *et al.* (Ref. 2) because there most of the electron trajectory was in regions where the potential experienced by the electron was almost flat so that the electron orbit was free to vary with the magnetic field.

[5] G. Timp *et al.*, Phys. Rev. Lett. **58**, 2814 (1987); K. Ishibashi *et al.*, Solid State Commun. **64**, 573 (1987); C. J. B. Ford *et al.*, Superlattices Microstruct. **4**, 541 (1988).

[6] Y. Takagaki and D. K. Ferry, Surf. Sci. **305**, 669 (1994); P. J.

Simpson *et al.*, *ibid.* **305**, 453 (1994); G. Kirczenow *et al.*, Phys. Rev. Lett. **72**, 2069 (1994); G. Kirczenow, Phys. Rev. B **50**, 1649 (1994).

[7] S. Ishizaka *et al.*, Phys. Rev. B **51**, 9881 (1995); K. Richter, Europhys. Lett. **29**, 7 (1995); T. Nakanishi and T. Ando, Phys. Rev. B **54**, 8021 (1996).

[8] See, G. Kirczenow, Phys. Rev. B **32**, 7952 (1985).

[9] Performing extensive quantum simulations such as those reported here using significantly finer lattices is not practical at present because of the limitations of computers.

[10] T. Usuki, M. Saito, M. Takatsu, R. A. Kiehl, and N. Yokoyama, Phys. Rev. B **52**, 8244 (1995).

[11] For a review see Y. Imry, in *Directions in Condensed Matter Physics*, edited by G. Grinstein and G. Masenko (World Scientific, Singapore, 1986), Vol. 1.

[12] E. Castaño and G. Kirczenow, Phys. Rev. B **41**, 5055 (1990).

[13] They were also observed when **B** was reversed.

[14] A similar collimation effect has been found by R. Akis, J. P. Bird, and D. K. Ferry, J. Phys.: Condens. Matter **8**, L667 (1996); R. Akis, D. K. Ferry, and J. P. Bird, Phys. Rev. B **54**, 17 705 (1996)

[15] We found several different closed classical orbits. The AB period behaved similarly for all of them.

[16] ΔB is stationary at the crossover and is thus observed experimentally to be constant there because the crossover is from a low B regime where ΔB decreases with increasing B to a high B regime where ΔB increases with increasing B, as is discussed in detail above.

[17] Y. Hirayama and T. Saku, Phys. Rev. B **42**, 11 408 (1990).